Sensitive dopamine sensor based on electrodeposited gold nanoparticles and electro-modulated MoS$_2$ nanoflakes

Qiufen Luo[1] · Yuan Su[1] · Hongfang Zhang[1]

Abstract

MoS$_2$ nanoflakes, though with graphene-like morphology, exhibit unsatisfactory performance in the fabrication of electrochemical sensors due to the poor conductivity. Herein, MoS$_2$ nanoflakes were electrochemically modulated, while gold nanoparticles (AuNPs) were co-electrodeposited by one-step cyclic voltammetry, forming a nanocomposite on the electrode surface. During the CV treatment, MoS$_2$ nanoflakes could be easily transformed from the original 2H phase with semiconductor properties to 1T phase with metal properties. The good electrical conductivity and also the big specific area of the ultimate AuNPs/1T-MoS$_2$ composite can be reflected by the CV and electrochemical impedance spectroscopy characterization. The nanocomposite exhibited attractive catalytic capacity to the electrochemical redox of dopamine (DA). Therefore, a DA sensor based on AuNPs/1T-MoS$_2$ was constructed. Using the detection technique of amperometry, the sensor displayed a wide linear range from 0.2 μmol/L to 1.0 mmol/L with low detection limit of 0.15 μmol/L. Using the detection technique of differential pulse voltammetry, the sensor demonstrated excellent selectivity when was applied in the sample containing excessive amount of ascorbic acid. Furthermore, the sensor could be used to detect dopamine in serum with a recovery rate of 106.5-109.4%.

Keywords Electrochemical sensor · MoS$_2$ nanoflakes · Gold nanoparticles · Dopamine

Introduction

Dopamine (DA) is the most abundant catecholamine neurotransmitter in the human brain. It plays an important role in physiological activities and thus regulates the activities of the central nervous system, hormones and cardiovascular system [1, 2]. When the systemic regulation of dopamine encounters obstacles, it may cause a variety of diseases, such as Parkinson's disease, schizophrenia, attention deficit, hyperactivity and pituitary tumors [3, 4]. Low or high levels of DA may be connected with the occurrence of these diseases. Therefore, detection of DA concentration in human body fluids is of great significance. At present, techniques for determining DA mainly include spectrometry [5], capillary electrophoresis [6] and electrochemical sensor

[7]. The o-hydroxy group on the DA benzene ring is prone to oxidation reaction on the electrode surface; therefore, the quantitative detection of DA can be realized by electrochemical analysis method [8, 9]. However, the detection of DA in clinical samples such as serum or urine is a great challenge. On the one hand, the content of DA is extremely low, which requires highly sensitive sensors. On the other hand, the electrochemical detection of DA is also susceptible to the interference of biological molecules with similar redox potentials such as ascorbic acid (AA) and uric acid (UA) [10, 11], which spawned the modification of composite nanomaterials to improve the surface performance of the electrode to eliminate the interference of small biological molecules such as AA.

At present, many functional materials, including metal nanoparticles [12], carbon nanomaterials [13] and polymers [14] have been used to prepare DA electrochemical sensors. MoS$_2$ nanoflakes also attracted the attention of researchers due to the stable chemical properties, good electronic mobility and layered structure similar to graphene [15, 16]. Due to the different order of S atoms, MoS$_2$ has two different crystalline phases, namely thermodynamically stable 2H

✉ Hongfang Zhang
zhanghf@nwu.edu.cn

1 Key Laboratory of Synthetic and Natural Functional Molecule Chemistry of the Ministry of Education, College of Chemistry & Materials Science, Northwest University, Xi'an 710127, Shaanxi, China

phase and metastable 1T phase. Metal-phase 1T-MoS$_2$ has higher conductivity and better charge transfer ability than semiconductor 2H-MoS$_2$ [17]. Chia et al. [18] proposed that MoS$_2$ nanoflakes could be transformed from 2H phase to 1T phase through electrochemical modulation, thereby improving the charge transfer ability and catalytic performance of MoS$_2$ nanoflakes. Furthermore, the conductivity and electrocatalytic performance of MoS$_2$ nanoflakes are enhanced by doping noble metal nanomaterials into MoS$_2$ nanoflakes [19]. Gold nanoparticles are considered as ideal materials for surface modification of MoS$_2$ due to their excellent conductivity and high stability [20]. Therefore, the analytical performance of the electrochemical sensor was further improved by doping AuNPs on the metal-phase 1T-MoS$_2$.

In this work, a novel electrochemical sensor based on AuNPs/1T-MoS$_2$ was constructed for the detection of dopamine (Fig. 1). The synergistic effect of 1T-MoS$_2$ nanoflakes and AuNPs ensures the conductivity, specific surface area and catalytic performance of the material, thus effectively promoting the electrochemical redox process of DA.

Experimental section

Chemicals and materials

MoS$_2$ nanoflakes were obtained from XFNANO (Nanjing, China). Gold(III) tetrachloride trihydrate (HAuCl$_4$ $\geq$ 47.8% as Au) was purchased from Shanghai Chemical Reagent Co., Ltd (China). DA, UA and AA were purchased from Xi'an Sanpu Chemical Reagent Co., Ltd (China). Phosphate-bufferd solution (PBS) was prepared using analytical grade chemicals KH$_2$PO$_4$ and Na$_2$HPO$_4$. Freshly prepared DA solution was used. All other reagents were analytical grade and used as received without further purification. All aqueous solutions were prepared with doubly distilled water.

Apparatus

All voltammetry experiments were carried out with a CHI440C electrochemical workstation (CH Instruments, China). A conventional three-electrode system with either a bare or modified glassy carbon electrode (GCE) as the working electrode, a saturated calomel electrode (SCE) as the reference electrode and a platinum wire as the counter electrode was applied. Scanning electron microscopy (SEM) and transmission electron microscopy (TEM) were obtained using a JSM-6390 A SEM (JEOL, Japan) and Tecnai G2F20 S-Twin (FEI, USA), respectively.
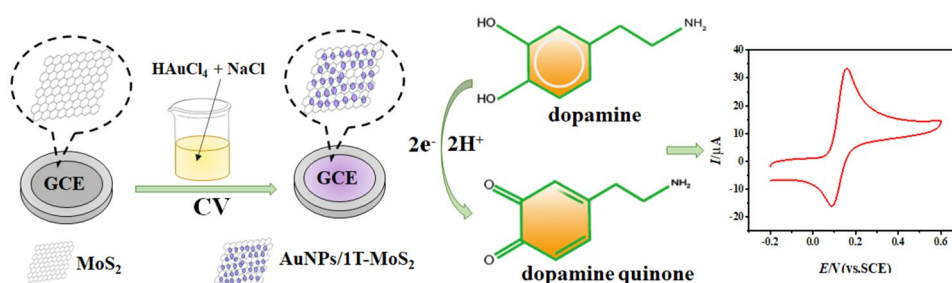
Preparation of AuNPs/1T-MoS$_2$/GCE

A bare GCE (3 mm in diameter) was mechanically polished with 0.3 and 0.05 μm alumina aqueous slurry. After ultrasonic washing in distilled water, 6 μL of 0.3 mg/mL dispersion of MoS$_2$ nanoflakes was cast on the GCE. After drying in air, MoS$_2$/GCE was acquired. AuNPs/1T-MoS$_2$/GCE was prepared by CV scanning in 0.5 mol/L NaCl solution containing 0.5 mmol/L HAuCl$_4$ (voltage: 1.1 to – 1.1 V, scan rate: 50 mV/s, 6 cycles). 1T-MoS$_2$/GCE and AuNPs/GCE were prepared in a similar way for comparison. 1T-MoS$_2$/GCE was the product of MoS$_2$/GCE after treated by CV scanning in 0.5 mol/L NaCl solution from 1.1 to – 1.1 V at a scan rate of 50 mV/s (6 cycles). AuNPs/GCE was prepared with the same CV procedure by immersing GCE in 0.5 mol/L NaCl solution containing 0.5 mmol/L HAuCl$_4$.

Electrochemical measurements

Electrochemical measurements were performed in 0.1 mol/L PBS (pH 7.0) solution using AuNPs/1T-MoS$_2$/GCE as working electrode. For amperometry, a working potential of 0.25 V was applied and DA was continuously injected in the solution under stirring after a short time for steady background current. For differential pulse voltammetry (DPV), DA was contained in 0.1 mol/L PBS (pH 7.0) solution and signal was recorded with potential range of – 0.2 to 0.6 V (pulse amplitude: 50 mV, pulse width: 50 ms, pulse period: 0.5 s).

Fig. 1 Construction and application of electrochemical sensor based on AuNPs/1T-MoS$_2$

Results and discussion

Characterization of AuNPs/1T-MoS$_2$/GCE

Morphology of MoS$_2$ nanoflakes was characterized by TEM and SEM. MoS$_2$ nanoflakes had typical lamellar nanostructures. Most of them displayed single layer and few are multilayer (Fig. 2A). The size of the nanosheet was irregular. Modification on the electrode surface (Fig. 2B) and the subsequent electrochemical modulation (Fig. 2C) did not change the morphology of the nanoflakes. After adding HAuCl$_4$ in the electrolyte solution, it was observed that a large number of gold nanoparticles with the average size of 50 nm were distributed on the MoS$_2$ nanoflakes (Fig. 2D), indicating the successful preparation of the AuNPs/1T-MoS$_2$/GCE.

The electron transfer property of AuNPs/1T-MoS$_2$/GCE was investigated by cyclic voltammetry and electrochemical impedance spectroscopy. As shown in Fig. 3A, modification of MoS$_2$ nanoflakes decreased the redox peak current of $[Fe(CN)_6]^{3-/4-}$, hinting the poor conductivity of the material. However, peak current obtained at 1T-MoS$_2$/GCE was 1.86 times as large as that of MoS$_2$/GCE. Due to the electrochemical pretreatment process, MoS$_2$ nanoflakes were transformed from the 2H phase with semiconductor property to the 1T phase with metal property

[18]. Therefore, electron transfer of the electrode surface was promoted after the electrochemical modulation. When Au nanoparticles were electrodeposited on the surface of 1T-MoS$_2$, the anodic and cathodic peak currents of ferricyanide obtained at AuNPs/1T-MoS$_2$/GCE were larger than those at 1T-MoS$_2$/GCE or AuNPs/GCE. These results illustrated that AuNPs/1T-MoS$_2$ possessed excellent electrical conductivity and big effective surface, due to the synergistic effect of the nanoflakes and the nanoparticles. These results were further verified by the electrochemical impedance spectroscopy for different electrodes. The diameter of the semicircle referred to the charge transfer resistance (R_{ct}) on the electrode surface. As shown in Fig. 3B, R_{ct} of 1T-MoS$_2$/GCE was smaller than that of MoS$_2$/GCE, indicating tuned electron-transfer kinetics of MoS$_2$-based film after phase transition. It can be also observed that the electron transfer hindrance at 1T-MoS$_2$/GCE is poorer when compared with the freshly polished GCE. As expected, R_{ct} of AuNPs/1T-MoS$_2$/GCE was significantly smaller than that of 1T-MoS$_2$/GCE, indicating that co-deposition of AuNPs onto the flakes of 1T-MoS$_2$ could further reduce the electron transfer resistance [21]. Therefore, the further integration of AuNPs is essential to the purpose of sensor fabrication.
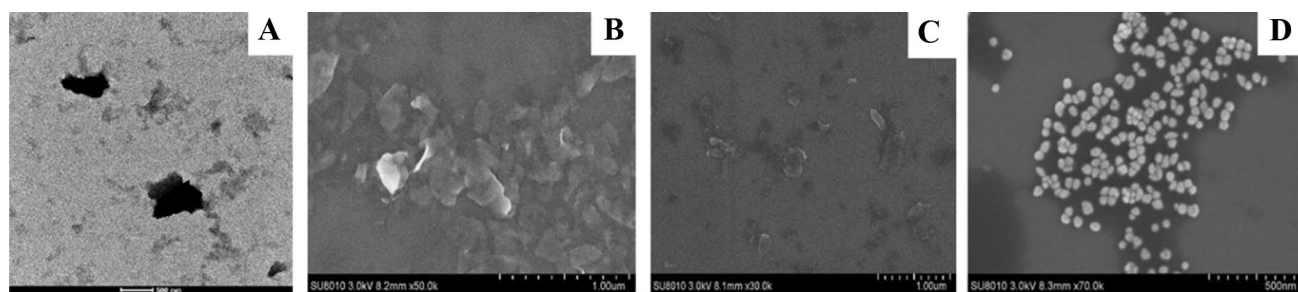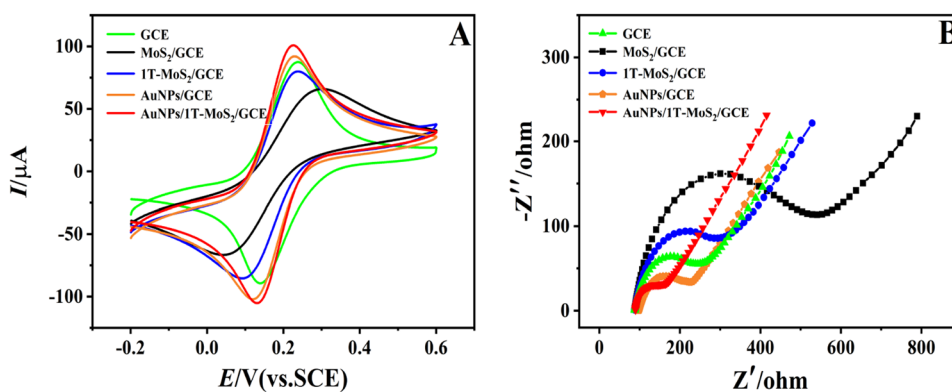

Fig. 2 TEM image of the MoS$_2$ nanoflakes (**A**), SEM image of the MoS$_2$ nanoflakes before (**B** and **C**) and after CV treatment as well as the co-deposited AuNPs (**D**)

Fig. 3 **A** CVs and **B** Nyquist plots of GCE, MoS$_2$/GCE, 1T-MoS$_2$/GCE, AuNPs/GCE and AuNPs/1T-MoS$_2$/GCE in 0.1 mol/L KCl solution containing 5 mmol/L $[Fe(CN)_6]^{3-/4-}$. Scan rate for CV is 100 mV/s

Voltammetry behavior of DA at AuNPs/1T-MoS₂/GCE

Voltammetric behavior of DA at bare GCE, MoS₂/GCE, 1T-MoS₂/GCE, AuNPs/GCE and AuNPs/1T-MoS₂/GCE were investigated in 0.1 mol/L PBS (pH 7.0) containing
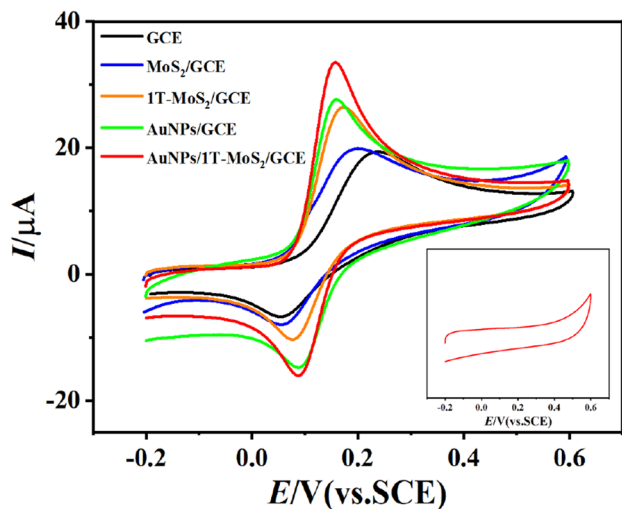

Fig. 4 CVs of GCE, MoS₂/GCE, 1T-MoS₂/GCE, AuNPs/GCE and AuNPs/1T-MoS₂/GCE in 0.1 mol/L PBS (pH 7.0) containing 1.0 mmol/L DA. Insert is the background signal of AuNPs/1T-MoS₂/GCE in 0.1 mol/L PBS (pH 7.0). Scan rate is 100 mV/s

1.0 mmol/L DA. As can be seen in Fig. 4, a pair of redox peaks could be observed at the voltammograms of all the electrodes. Compared with it for the bare electrode, the redox peak current on MoS₂/GCE increased slightly. This might be attributed to the modification of layered MoS₂ nanoflakes, which increased the effective surface area for DA redox. After electrochemical modulation, the redox peak current of DA increased significantly, indicating that the high conductivity of 1T-MoS₂ is conducive to the electrode reaction of DA. After gold nanoparticles deposition, the oxidation peak current reached 1.82 times of that obtain at bare electrode, demonstrating the synergistic catalysis of 1T-MoS₂ and gold nanoparticles. These results illustrated that AuNPs/1T-MoS₂/GCE could be used for sensitive DA detection.

Effect of scan rate

The voltammetric behavior of dopamine at AuNPs/1T-MoS₂/GCE was further investigated. As revealed by Fig. 5A, the redox peak current of DA increased with increasing scan rate in the range of 20–300 mV/s. The anodic ($R^2 = 0.993$) and cathodic ($R^2 = 0.995$) peak currents were linearly proportional to the square root of the scan rate, indicating a typical diffusion-controlled electrochemical process. In addition, the redox peak potentials (E_{pa} and E_{pc}) provided a linear relationship with ln v (Fig. 5C). Thus, the electron transfer

Fig. 5 **A** Cyclic voltammograms of AuNPs/1T-MoS₂/GCE in 0.1 M PBS (pH 7.0) containing 1.0 mM DA with different scan rate (20–300 mV s⁻¹). **B** Relationship of oxidation and reduction peak potential (E_{pa} and E_{pc}) versus ln v. **C** CVs of AuNPs/1T-MoS₂/GCE in 0.1 mol/L PBS (pH 7.0) containing 1.0 mmol/L DA at various pH PBS (pH 5.0, 6.0, 7.0, 8.0 and 9.0), respectively, scan rate 100 mV/s. **D** Linear relationship of oxidation and reduction peak potential (E_{pa} and E_{pc}) versus pH
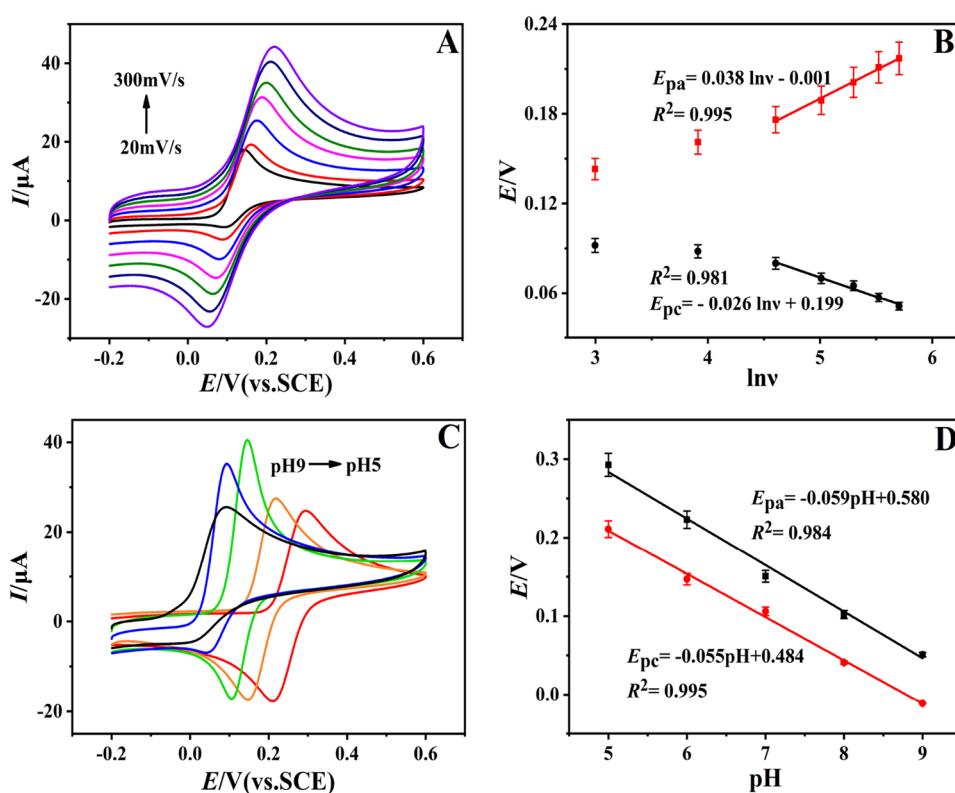
number involved in the redox reaction of DA can be calculated according to the Laviron's equation (Eqs. 1, 2) [22]. The electron transfer coefficient (α) and the electron transfer number (n) were calculated to be 0.58 and 1.96, respectively. Then, it can be concluded that the electrochemical mechanism of DA redox at the surface of AuNPs/1T-MoS$_2$/GCE still follows a two-electron process [23]:

$$E_{pa} = E^{0'} + \frac{RT}{(1-\alpha)nF} \ln \upsilon \tag{1}$$

$$E_{pc} = E^{0'} - \frac{RT}{\alpha nF} \ln \upsilon \tag{2}$$

Effect of pH value

The electrochemical redox behavior of DA at AuNPs/1T-MoS$_2$/GCE in buffer system in the pH range of 5.0–9.0 was investigated by CV. As can be seen from Fig. 5C, the peak current of DA increased and then decreased with the increase in pH, reaching the maximum at pH 7.0. In mildly acidic condition, the electrochemical process may be influenced by the protonation of the amino groups of DA. Under weakly alkaline condition, DA became auto-oxidized and polydopamine was finally formed after a series of reactions [24, 25]. Therefore, pH 7.0 was consequently selected for electrochemical DA detection in the following experiments.

The redox peak potentials (E_{pa} and E_{pc}) of dopamine shifted negatively with the increase in pH, indicating the proton-coupled nature of DA electrochemical redox. The linear relationship between redox peak potentials and pH was shown in Fig. 5D. The slope value of -0.059 V/pH and -0.055 V/pH was very close to the Nernstian value of -0.059 V/pH, indicating that the number of electrons and protons involved in the oxidation reaction was equal. Therefore, it manifested that there are two protons and two electrons involved in the electrochemical redox reaction of DA [26]. As illustrated in Fig. 1, DA is converted to its quinone form.

Electrochemical determination of DA

Amperometric determination of DA

Amperometric technique was applied to the quantification of DA for its high sensitivity and rapid response. The working potential was optimized to acquire better performance at the sensor. Figure 6A illustrated that the current response increased gradually with the increase in working potential in the range of 0.10–0.30 V, and the maximum current response appeared at the applied potential of 0.30 V. However, the current response obtained at 0.30 V was less stable. Therefore, 0.25 V was selected as the optimal working potential. Figure 6B displayed the amperometric response of AuNPs/1T-MoS$_2$/GCE when DA was continuously added into 0.1 mol/L PBS (pH 7.0) with continuous

Fig. 6 **A** Amperometric response obtained at AuNPs/1T-MoS$_2$/GCE for successive addition of 0.01 mmol/L DA into 0.1 mol/L PBS (pH = 7.0) at various applied potentials. **B** Amperometric curve obtained at AuNPs/1T-MoS$_2$/GCE with addition of DA in PBS (pH 7.0) at 0.25 V. **C** Plot of oxidation peak currents derived from amperometric curve versus DA concentrations. **D** Amperometric response obtained at AuNPs/1T-MoS$_2$/GCE for successive addition of 2.0 mmol/L DA, 2.0 mmol/L NaCl, KCl, CaCl$_2$, glucose, 1.0 mmol/L AA and UA into 0.1 mol/L PBS (pH 7.0)
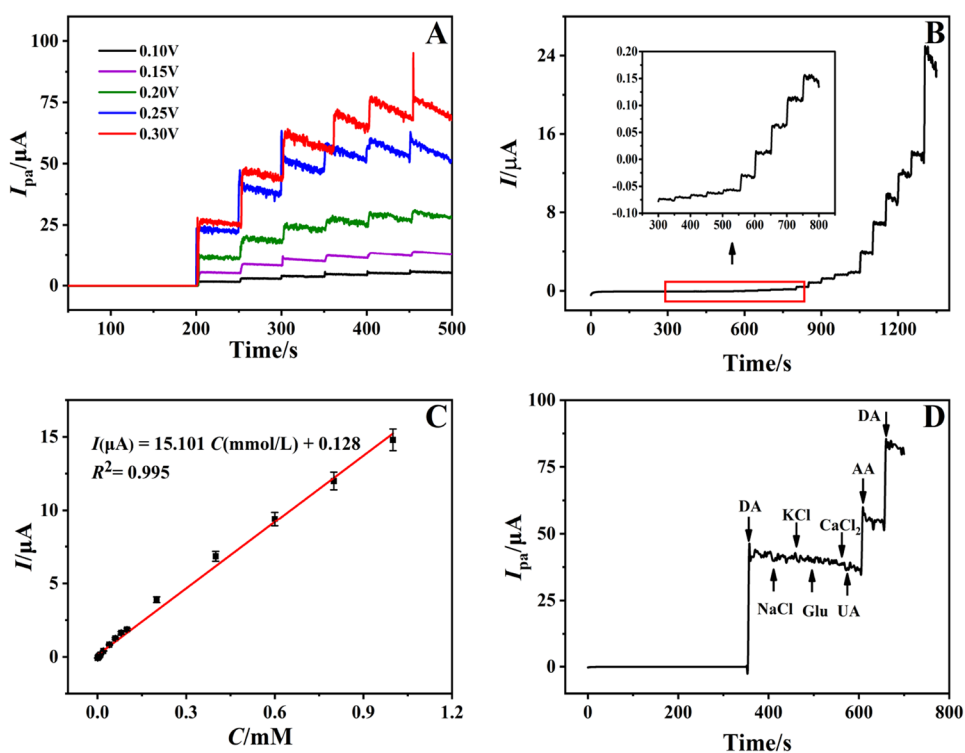
stirring at working potential of 0.25 V. As can be seen, the peak current of DA increased linearly with the increase in DA concentration in the broad range of 0.2–1000 µmol/L (Fig. 6C). The corresponding regression equation was I_{pa} (µA) $= 15.101C$ (mmol/L) $+ 0.128$ with a correlation coefficient of 0.995. The limit of detection was estimated to be 0.15 µmol/L according to the principle of 3 s/b (s represents the standard deviation of blank solution and b represents the slope of calibration curve).

Selectivity was the most important evaluation index for an electrochemical DA sensor because of the fact that the serum coexistence AA and UA are both electroactive. As shown in Fig. 6D, the current response was not obvious after injection of 2 mmol/L NaCl, KCl, $CaCl_2$ and glucose. The influence of the above interfering substances on the determination of DA could be ignored. However, the addition of 1 mmol/L AA produced a significant response at the amperometric I–t curve, demonstrating that the interference of AA cannot be avoided.

Differential pulse voltammetric determination of DA

DPV is also a sensitive electrochemical technique that can reduce the effect of capacitive current and improves the signal-to-noise ratio. What is more, the peak-shaped response of DPV makes it possible to yield obvious peak separation between DA and excessive amounts of

the interferences like AA. Therefore, the electrochemical behavior of DA at AuNPs/1T-MoS₂/GCE was further studied by DPV. Figure 7A demonstrates the response for different DA concentrations in 0.1 mol/L PBS (pH 7.0) solution. As expected, DPV results illustrated that the anodic peak current increased as the DA concentration increased from 0.2 to 80 µmol/L. The plot of oxidation peak current (I_{pa}) versus DA concentration (c) exhibited two linear ranges. The linear relationships could be expressed by the regression equation I_{pa} (µA) $= 0.146C$ (µmol/L) $+ 0.146$ ($R^2 = 0.995$, $0.20{-}10$ µmol/L), I_{pa} (µA) $= 0.069C$ (µmol/L) $+ 0.919$ ($R^2 = 0.996$, $10{-}80$ µmol/L) (Fig. 7B). The limit of detection was estimated to be 0.16 µmol/L.

Figure 7C shows that the AuNPs/1T-MoS₂ modified electrode exhibited good selectivity for DA detection in the presence of AA. The oxidation potential of AA and DA was -0.041 V and 0.15 V, which could be effectively separated by DPV. The oxidation peak current acquired at AuNPs/1T-MoS₂/GCE in 0.1 mol/L PBS (pH 7.0) containing 40 µmol/L DA and 20 µmol/L AA only changed 2.0% when compared with it in 0.1 mol/L PBS (pH 7.0) containing 40 µmol/L DA without AA. Therefore, the sensor can be applied to DA detection in the sample containing excessive amount of ascorbic acid.

What is more, good reproducibility and stability were crucial for electrochemical sensors. Five AuNPs/1T-MoS₂/

Fig. 7 **A** DPV response for different concentrations of DA (0.2, 0.4, 0.6, 0.8, 1.0, 2.0, 4.0, 6.0, 8.0, 10, 20, 40 and 80 µmol/L) obtained at AuNPs/1T-MoS₂/GCE. **B** Plot of peak current derived from DPV versus DA concentration. **C** DPV response of AuNPs/1T-MoS₂/GCE in 0.1 M PBS (pH 7.0) containing 40 µmol/L DA and 20 µmol/L AA. **D** The measurement results obtained at 5 AuNPs/1T-MoS₂/GCEs
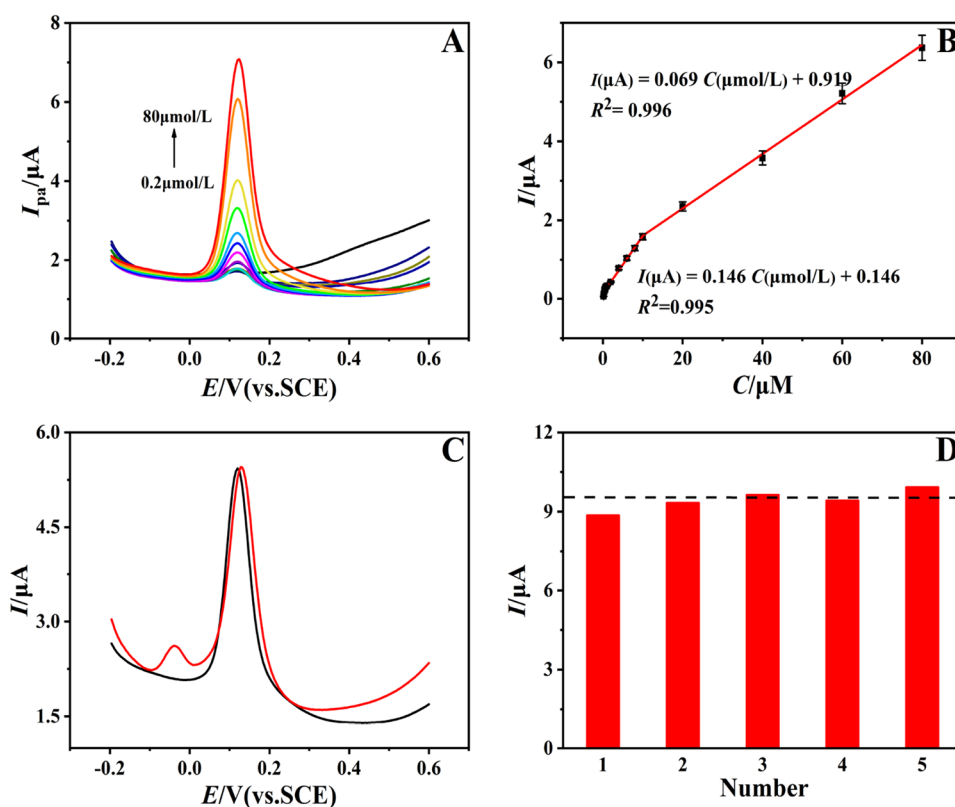
Table 1 Comparison of analytical performance of different DA sensors

Modified electrodes	Method	Linear range(μM)	Detection limit (μM)	References
AuNPs/PPy/GCE	DPV	0.75–20	0.15	[27]
MoS_2/PEDOT/GCE	DPV	1–80	0.52	[28]
MoS_2/rGO/GCE	DPV	1.5–100	0.94	[29]
AuNPs@PANI/GSPE	DPV	1–100	0.86	[30]
CNT/PFS/GCE	Amperometry	0.8–61	0.20	[31]
$Zn–Co_2O_4$/GCE	Amperometry	0.2–185	0.002	[32]
$Cu_2O@g–C_3N_4$/GCE	Amperometry	0.025–910	0.045	[33]
$PtAg/WS_2$/GCE	Amperometry	0.6–1000	0.2	[34]
AuNPs/$1T-MoS_2$/GCE	Amperometry	0.2–1000	0.15	This work
AuNPs/$1T-MoS_2$/GCE	DPV	0.2–80	0.16	This work

PPy is polypyrrole, *GSPE* is graphite screen-printed electrodes, and *PFS* is polymeric ferric sulfate

GCE were prepared in the same way, and their response for DA was shown in Fig. 7D. The relative standard deviation (RSD) was calculated to be 4.2%, suggesting an acceptable reproducibility. The prepared sensor was stored at 4 °C for 15 days to test its stability. The peak current for 20 μmol/L DA decreased to 91.1% of its initial response, indicating the good stability of the sensor based on AuNPs/$1T-MoS_2$.

The electrochemical performance of this sensor was compared with it of some other DA sensors. From Table 1, it was obvious that the sensor exhibited a wide linear working range as well as low detection limit.

Analytical application

The analytical application of AuNPs/$1T-MoS_2$/GCE was investigated by detecting DA in human serum. The serum was diluted 10 times with 0.1 mol/L PBS (pH 7.0). Using the technique of DPV, recoveries were obtained by the standard addition method. The results are summarized in Table 2. The recovery for spiked DA with three different concentration levels was 109.0%, 109.4% and 106.5%, respectively. The results illustrated that AuNPs/$1T-MoS_2$/GCE was reliable and effective for the determination of DA.

Conclusions

In this work, a DA sensor was developed based on the composite of AuNPs and MoS_2 nanoflakes. The simple drop-casting and CV scanning process not only formed AuNPs/MoS_2 nanocomposite, but also transformed the 2H

Table 2 Determination results of DA in serum ($n = 3$)

Sample number	Added (μmol/L)	Found (μmol/L)	Recovery (%)	RSD (%)
1	2.0	2.2	109.0	2.4
2	20.0	21.9	109.4	3.1
3	40.0	42.6	106.5	6.2

semiconductor phase MoS_2 to 1T metal-phase counterpart. The excellent conductivity and the big specific surface area of the composite resulted in a sensitive electrochemical sensor for DA detection. Both amperometry and DPV measurements demonstrated the wide linear range and low detection limit of the sensor. Furthermore, the interference of the other biological species like AA could be avoided via the DPV measurement. The recovery tests provide a broad prospect for the determination of DA in human body fluids.

Declarations

References

1. J.D. Berke, Nat. Neurosci. **21**, 787–793 (2018)
2. N.D. Volkow, R.A. Wise, R. Baler, Nat. Rev. Neurosci. **18**, 741–752 (2017)
3. V. Voon, T.C. Napier, M.J. Frank, V. Sgambato-Faure, A.A. Grace, M. Rodriguez-Oroz, J. Obeso, E. Bezard, P.O. Fernagut, Lancet Neurol. **16**, 238–250 (2017)
4. K. Wang, L. Dong, X. Zhang, X. Wang, Chem. Life **34**, 184–192 (2014)
5. A. Naccarato, E. Gionfriddo, G. Sindona, A. Tagarelli, Anal. Chim. Acta. **810**, 17–24 (2014)
6. A. Bacaloni, S. Insogna, A. Sancini, M. Ciarrocca, F. Sinibaldi, Biomed. Chromatogr. **27**, 987–993 (2013)
7. F. Foroughi, M. Rahsepar, H. Kim, J. Electroanal. Chem. **827**, 34–41 (2018)
8. C. Yang, M.E. Denno, P. Pyakurel, B.J. Venton, Anal. Chim. Acta. **887**, 17–37 (2015)
9. M. Kumar, B.E.K. Swamy, S. Reddy, W. Zhao, S. Chetana, V.G. Kumar, J. Electroanal. Chem. **835**, 96–105 (2019)

10. M. Noroozifar, M. Khorasani-Motlagh, R. Akbari, M. Bemanadi Parizi, Biosens. Bioelectron. **28**, 56–63 (2011)

11. T. Palomaki, E. Peltola, S. Sainio, N. Wester, O. Pitkanen, K. Kordas, J. Koskinen, T. Laurila, Biosens. Bioelectron. **123**, 281–284 (2019)

12. X. Liu, Y. Fu, Q. Sheng, J. Zheng, Microchem. J. **146**, 509–516 (2019)

13. Q. Huang, X. Lin, L. Tong, Q.-X. Tong, A.C.S. Sustain, Chem. Eng. **8**, 1644–1650 (2020)

14. N. Ermiş, N. Tinkiliç, Electroanalysis **33**, 1491–1501 (2021)

15. K. Silambarasan, J. Archana, S. Harish, M. Navaneethan, R. Sankar Ganesh, S. Ponnusamy, C. Muthamizhchelvan, K. Hara, J. Mater. Sci. Technol. **51**, 94–101 (2020)

16. K.-J. Huang, L. Wang, J. Li, Y.-M. Liu, Sens. Actuators B Chem. **178**, 671–677 (2013)

17. M. Acerce, D. Voiry, M. Chhowalla, Nat. Nanotechnol. **10**, 313–318 (2015)

18. X. Chia, A. Ambrosi, D. Sedmidubsky, Z. Sofer, M. Pumera, Chem. Eur. J. **20**, 17426–17432 (2014)

19. L.H. Yuwen, F. Xu, B. Xue, Z.M. Luo, Q. Zhang, B.Q. Bao, S. Su, L.X. Weng, W. Huang, L.H. Wang, Nanoscale **6**, 5762–5769 (2014)

20. N. Elahi, M. Kamali, M.H. Baghersad, Talanta **184**, 537–556 (2018)

21. T. Liang, J.-H. Cao, W.-H. Liang, Q. Li, L. He, D.-Y. Wu, RSC Adv. **9**, 41151 (2019)

22. E. Laviron, J. Electroanal. Chem. Interfacial Electrochem. **101**, 19–28 (1979)

23. C. Li, J. Zhao, X. Yan, Y. Gu, W. Liu, L. Tang, B. Zheng, Y. Li, R. Chen, Z. Zhang, Analyst **140**, 1913–1920 (2015)

24. M. Salomäki, L. Marttila, H. Kivelä, T. Ouvinen, J. Lukkari, J. Phys. Chem. B. **122**, 6314–6327 (2018)

25. W. Cheng, X. Zeng, H. Chen, Z. Li, W. Zeng, L. Mei, Y. Zhao, ACS Nano **13**, 8537–8565 (2019)

26. S. Schindler, T. Bechtold, J. Electroanal. Chem. **836**, 94–101 (2019)

27. J. Li, X. Lin, Sens. Actuators B Chem. **124**, 486–493 (2007)

28. Y. Li, H. Lin, H. Peng, R. Qi, C. Luo, Microchim. Acta. **183**, 2517–2523 (2016)

29. K. Pramoda, K. Moses, U. Maitra, C.N.R. Rao, Electroanalysis **27**, 1892–1898 (2015)

30. G. Selvolini, C. Lazzarini, G. Marrazza, Sensors **19**, 3097 (2019)

31. T. Ni, T. Wang, L. Xi, Anal. Lett. **50**, 1730–1742 (2017)

32. M.I. Khan, N. Muhammad, M. Tariq, U. Nishan, A. Razaq, T.A. Saleh, M. Abu Haija, I. Ismail, A. Rahim, Microchim. Acta. **189**, 37 (2022)

33. U. Rajaji, S.V. Selvi, S.-M. Chen, S. Chinnapaiyan, T.-W. Chen, M. Govindasamy, Microchim Acta. **187**, 459 (2020)

34. Y. Li, C. Fan, J. Zheng, J. Mater. Sci. Mater. Electron. **33**, 5061–5072 (2022)